RNA (2002), *8*:29–46. Cambridge University Press. Printed in the USA.

DOI: 10.1017.S1355838201014066

Structure of the histone mRNA hairpin required for cell cycle regulation of histone gene expression

KATIA ZANIER,[1] INGRID LUYTEN,[1] CATRIONA CROMBIE,[2] BERNDT MÜLLER,[2] DANIEL SCHÜMPERLI,[3] JENS P. LINGE,[1,4] MICHAEL NILGES,[1,4] and MICHAEL SATTLER[1]

[1]Structural and Computational Biology, European Molecular Biology Laboratory, Heidelberg, Germany
[2]Department of Molecular and Cell Biology, Institute of Medical Sciences, University of Aberdeen, Aberdeen AB25 2ZD, Scotland, United Kingdom
[3]Institute of Cell Biology, University of Bern, 3012 Bern, Switzerland

ABSTRACT

Expression of replication-dependent histone genes requires a conserved hairpin RNA element in the 3′ untranslated regions of poly(A)-less histone mRNAs. The 3′ hairpin element is recognized by the hairpin-binding protein or stem-loop-binding protein (HBP/SLBP). This protein–RNA interaction is important for the endonucleolytic cleavage generating the mature mRNA 3′ end. The 3′ hairpin and presumably HBP/SLBP are also required for nucleocytoplasmic transport, translation, and stability of histone mRNAs. RNA 3′ processing and mRNA stability are both regulated during the cell cycle. Here, we have determined the three-dimensional structure of a 24-mer RNA comprising a mammalian histone RNA hairpin using heteronuclear multidimensional NMR spectroscopy. The hairpin adopts a novel UUUC tetraloop conformation that is stabilized by base stacking involving the first and third loop uridines and a closing U-A base pair, and by hydrogen bonding between the first and third uridines in the tetraloop. The HBP interaction of hairpin RNA variants was analyzed in band shift experiments. Particularly important interactions for HBP recognition are mediated by the closing U-A base pair and the first and third loop uridines, whose Watson–Crick functional groups are exposed towards the major groove of the RNA hairpin. The results obtained provide novel structural insight into the interaction of the histone 3′ hairpin with HBP, and thus the regulation of histone mRNA metabolism.

Keywords: hairpin; hairpin-binding protein; histone gene expression; isotope labeling; NMR; stem-loop-binding protein; structure

INTRODUCTION

The events that control mRNA metabolism of replication-dependent histone genes are unique among RNA polymerase II transcripts. The expression of these genes is coordinated with DNA synthesis and increases during the S-phase of the cell cycle (Schümperli, 1988; Osley, 1991) and control at the posttranscriptional level is essential for correct histone gene expression. The RNA hairpin element in the 3′ untranslated region (3′ UTR) of histone mRNA is required for this regulation and is involved in histone RNA 3′ end formation in the nucleus (Birchmeier et al., 1983; Mowry et al., 1989; Streit et al., 1993; Pandey et al., 1994). It is also required for export of the histone mRNA (Eckner et al., 1991; Williams et al., 1994), translation (Gallie et al., 1996) and the reduction of mRNA stability in response to the stoppage of DNA synthesis (Pandey & Marzluff, 1987). Remarkably, these functions are affected by point mutations at conserved positions in the hairpin sequence (Pandey et al., 1994; Williams et al., 1994; Gallie et al., 1996), highlighting the importance of the RNA hairpin element. The formation of the mRNA 3′ end is the best understood posttranscriptional processing event in the regulation of histone gene expression. It occurs by site-specific cleavage of the histone RNA between the 3′ hairpin element and a purine-rich spacer or histone downstream element located 11 to 12 nt 3′ of the cleavage site (Fig. 1A; Marzluff, 1992; Müller & Schümperli, 1997; Dominski & Marzluff, 1999).

Reprint requests to: Michael Sattler, European Molecular Biology Laboratory, Meyerhofstrasse 1, 69117 Heidelberg, Germany; e-mail: sattler@EMBL-Heidelberg.de.
[4]Present address: Unité de Bioinformatique Structurale, Institut Pasteur, 25–28 rue du docteur Roux, F-75015 Paris, France.

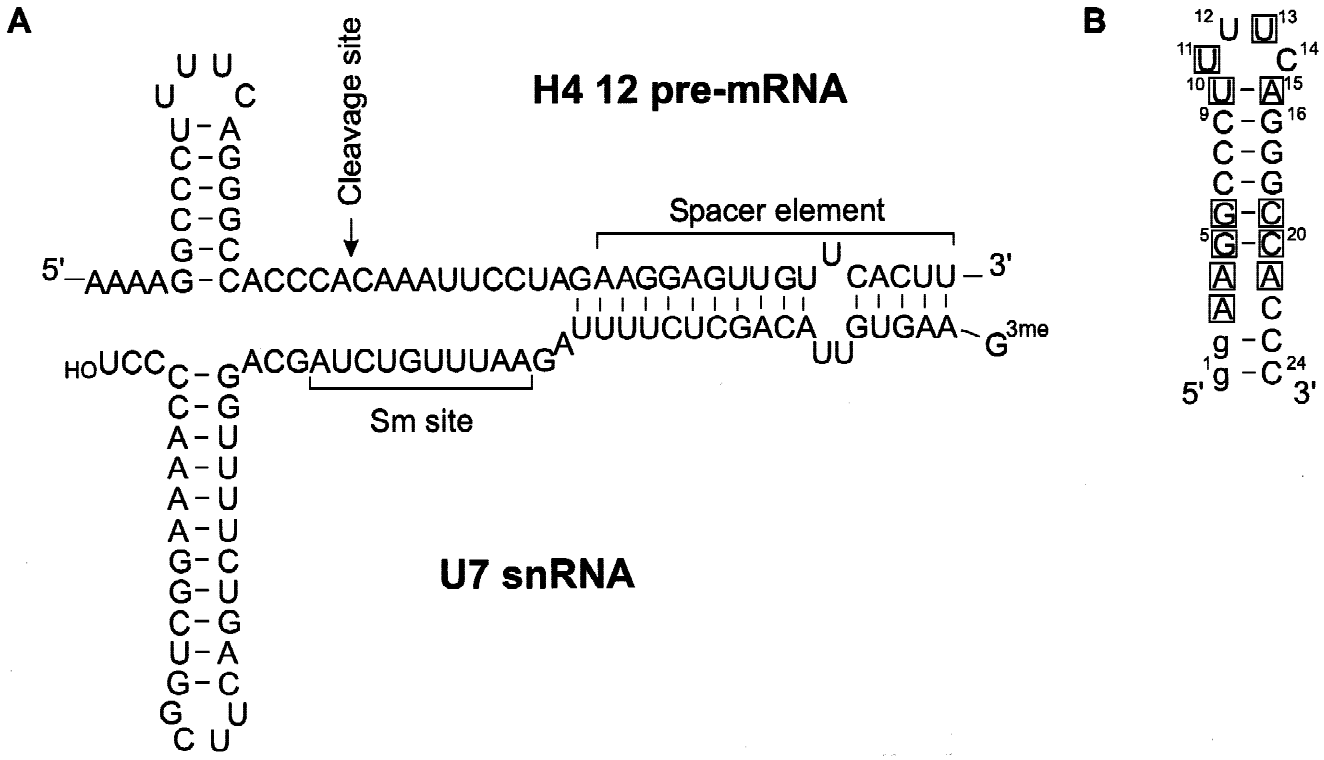

FIGURE 1. A: RNA/RNA interactions involved in histone pre-mRNA processing. Shown are the sequences of the 3′ UTR of mouse H4 12 histone gene and of the mouse U7 snRNA (Spycher et al., 1994). The potential of the 5′ end of the U7 snRNA to base pair with the spacer element is depicted. **B:** The 24-mer RNA construct used for the structure determination by NMR and in HBP binding studies. Conserved residues are boxed.

Histone RNA 3′ end formation is dependent on at least two *trans*-acting factors: (1) the hairpin-binding protein or stem-loop-binding protein (HBP/SLBP); and (2) the U7 small nuclear ribonucleoprotein (snRNP). U7 snRNP is targeted to the cleavage site by base pairing of the U7 snRNA 5′ end to the spacer element (Schaufele et al., 1986; Cotten et al., 1988; Bond et al., 1991). HBP/SLBP (referred to as HBP from here on; Wang et al., 1996; Martin et al., 1997) binds specifically to the histone 3′ hairpin structure (Dominski et al., 1999; Martin et al., 2000; Michel et al., 2000; Battle & Doudna, 2001) and is most likely involved in cell cycle regulation of histone RNA 3′ end formation. This is based on the observations that (1) similar to histone mRNA levels, HBP levels are cell-cycle regulated (Whitfield et al., 2000); (2) HBP is required for efficient RNA processing (Wang et al., 1996; Martin et al., 1997); and (3) HBP stabilizes the interaction of U7 snRNP with histone RNA (Dominski et al., 1999). It is assumed that HBP remains associated with the 3′ end of histone mRNA after maturation and that it may be involved in subsequent post-transcriptional regulation events that are dependent on the histone hairpin sequence. HBPs contain a conserved region of ~73 amino acids that is sufficient for RNA recognition (Wang et al., 1996; Michel et al., 2000). Neither this RNA-binding domain nor the full-length HBP are homologous to any described RNA-binding protein. Thus, the HBP–hairpin complex is expected to represent a novel type of protein–RNA recognition. In the histone 3′ hairpin element, the G5-C20, G6-C19, and U10-A15 base pairs, as well as U11 and U13 are conserved (Fig. 1B). Only in nematodes is U11 replaced by a cytosine (Marzluff, 1992; Wittop Koning & Schümperli, 1994). Notably, this substitution is crucial for the interaction of *Caenorhabditis elegans* HBP with this RNA hairpin (Michel et al., 2000). In vertebrates, also the nucleotides AA and AC flanking the stem at the 5′ and 3′ site, respectively, are conserved. In contrast, the bases at positions 12 and 14 in the loop are more variable.

Here, we have used heteronuclear dimensional nuclear magnetic resonance (NMR) to determine the three-dimensional structure of the histone RNA hairpin of the mouse histone H4-12 gene (Gruber et al., 1990; Fig. 1B). The 24-mer RNA molecule used for the structural studies comprises a hairpin sequence that is necessary and sufficient for HBP binding. The RNA hairpin adopts a novel tetraloop conformation that consists of four unpaired pyrimidine bases. We investigate the importance of loop residues for HBP binding in band shift assays. Our results suggest that HBP may specifically recognize conserved nucleotides that are exposed in the major groove of the histone 3′ mRNA hairpin.

RESULTS

Chemical shift assignments and structure determination

The 24-mer RNA (Fig. 1) used for the structural studies is sufficient to mediate high-affinity binding to HBP (Fig. 7 and data not shown). RNA samples were melted and snap-cooled to avoid potential dimerization of the 24-mer sequence. Based on analytical ultracentrifugation, native PAGE analysis, and a novel NMR-based method (see Materials and Methods), the 24-mer RNA adopts a monomeric hairpin conformation in solution. Addition of Mg^{2+} does not affect the NMR spectra, suggesting that the hairpin conformation is independent of divalent cations. Sample conditions were evaluated based on the imino resonances. NMR spectra at low salt concentrations (Na^+ or K^+) are comparable and exhibit narrow line widths, whereas salt concentrations $>$50 mM Na^+ causes line-broadening of the imino resonances. Therefore, a low salt buffer (10 mM sodium phosphate) was used for the structural studies. The base pairs in the stem were established by the HNN-COSY experiment (Fig. 2A; Dingley & Grzesiek, 1998). The $^{2h}J_{NN}$ coupling constants for the C-G base pairs (6.9–7.8 Hz) are comparable to previous reports of these couplings in canonical A-helical RNA stems (Dingley & Grzesiek, 1998). In contrast, the U10 imino proton gives rise to a very broad signal at the chemical shift expected for a U-A base pair (Fig. 2A), and this signal was not visible in NOESY or the HNN-COSY experiments. The coupling between the U10 N3 and the A15 N1 ($^{2h}J_{NN}$ = 5.6 Hz) was measured in experiments that detect nonexchangeable base protons (Hennig & Williamson, 2000; Fig. 2B) and is notably smaller compared to U-A base pairs in A-form RNA helices (Dingley & Grzesiek, 1998; Luy & Marino, 2000). The smaller $^{2h}J_{NN}$ coupling and the line-broadening of the U10 imino resonance suggest that the U10-A15 base pair is less stable and may be affected by small amplitude fluctuations resulting in "breathing" of this base pair (Luy & Marino, 2000). Taken together, the observed hydrogen bond pattern establishes that the hairpin RNA adopts a stem-loop structure with a tetraloop that is closed by a U-A base pair.

Standard homo- and heteronuclear NMR experiments were used for chemical shift assignments and to generate distance and torsion angle restraints (Varani et al., 1996; Wijmenga & van Buuren, 1998). Chemical shift assignments of the sugar and base spin systems were obtained as described in Materials and Methods. The majority of the stem residues were sequentially assigned from the regular sugar-base NOE patterns observed in three-dimensional ^{13}C-edited HMQC-NOESY spectra (Figs. 2 and 3). The H1′ to H6/H8 NOE walk traced in the anomeric-aromatic region of a two-dimensional NOESY spectrum is shown in Figure 2C. NOE-based sequential assignments for the loop and closing base pair residues are confirmed in ^1H, ^{31}P, and ^{13}C, ^{31}P through-bond experiments (Fig. 2D). Almost complete chemical shift assignments were obtained for the hairpin RNA (Table A1 in the Appendix).

Experimental torsion angle restraints for the sugar puckers were derived from homonuclear ^1H,^1H couplings measured in HCCH-E.COSY experiments (Schwalbe et al., 1995; Zimmer et al., 1996). The backbone angle γ and stereospecific assignments for H5′ and H5″ were obtained as described (Marino et al., 1996). The backbone angle ϵ was defined based on $^3J_{C2'P}$ couplings (Legault et al., 1995) and qualitative analysis of C4′, P cross-peak intensities in HCP experiments. Because all NMR data for residues 5–10 and 15–20 are in agreement with a canonical A-helical RNA conformation, Watson–Crick hydrogen bond distance and torsion angle restraints for standard A-form RNA were applied during the structure calculations. For the loop and closing base pair (U10-A15) residues, only NMR-derived torsion angle restraints were used (Table A2 in the Appendix).

Structures were calculated with an extended molecular dynamics/simulated annealing (MD/SA) protocol using ARIA/CNS (Linge et al., 2001). The quality of the ensemble of structures was assessed by back-calculating interresidue proton–proton distances and comparing them to the experimental NOE data. In some structures, alternative orientations were found for the bases of U11 or C14. However, these structures are not consistent with the experimental data, as they exhibit a number of short proton–proton distances for which no NOEs cross-peaks are observed in the NMR spectra, and were therefore excluded from the structure ensemble. The NMR structures obtained with ARIA/CNS were refined by restrained MD/SA in AMBER using a Generalized Born model for electrostatic interaction terms (Case et al., 1999). The final ensemble of NMR structures is in good agreement with the distance and torsion angle restraints. Structural statistics are summarized in Table 1. The region between G5 and C20 in the 24-mer RNA is well defined by the NMR data, with an average of $\sim$7/21 interresidual/total distance and $\sim$8 torsion angle restraints per residue. The heavy atom root mean square (rms) deviation is 0.79 Å for the family of the 15 lowest energy structures (Table 1; Fig. 4). The internal loop consisting of residues A3, A4, A21, and C22 is instead poorly defined due to the lack of cross-strand NOE contacts. The absence of pH-dependent chemical shift variations for the adenine C2-H2 group (not shown) is consistent with the lack of a potential $A3^+$-C22 base pair (Legault & Pardi, 1994). The relative orientations of the stem regions before and after this internal loop are not well defined with respect to each other. Therefore, in the following only the conformation of the stem-loop comprising residues 5 to 20 is discussed.

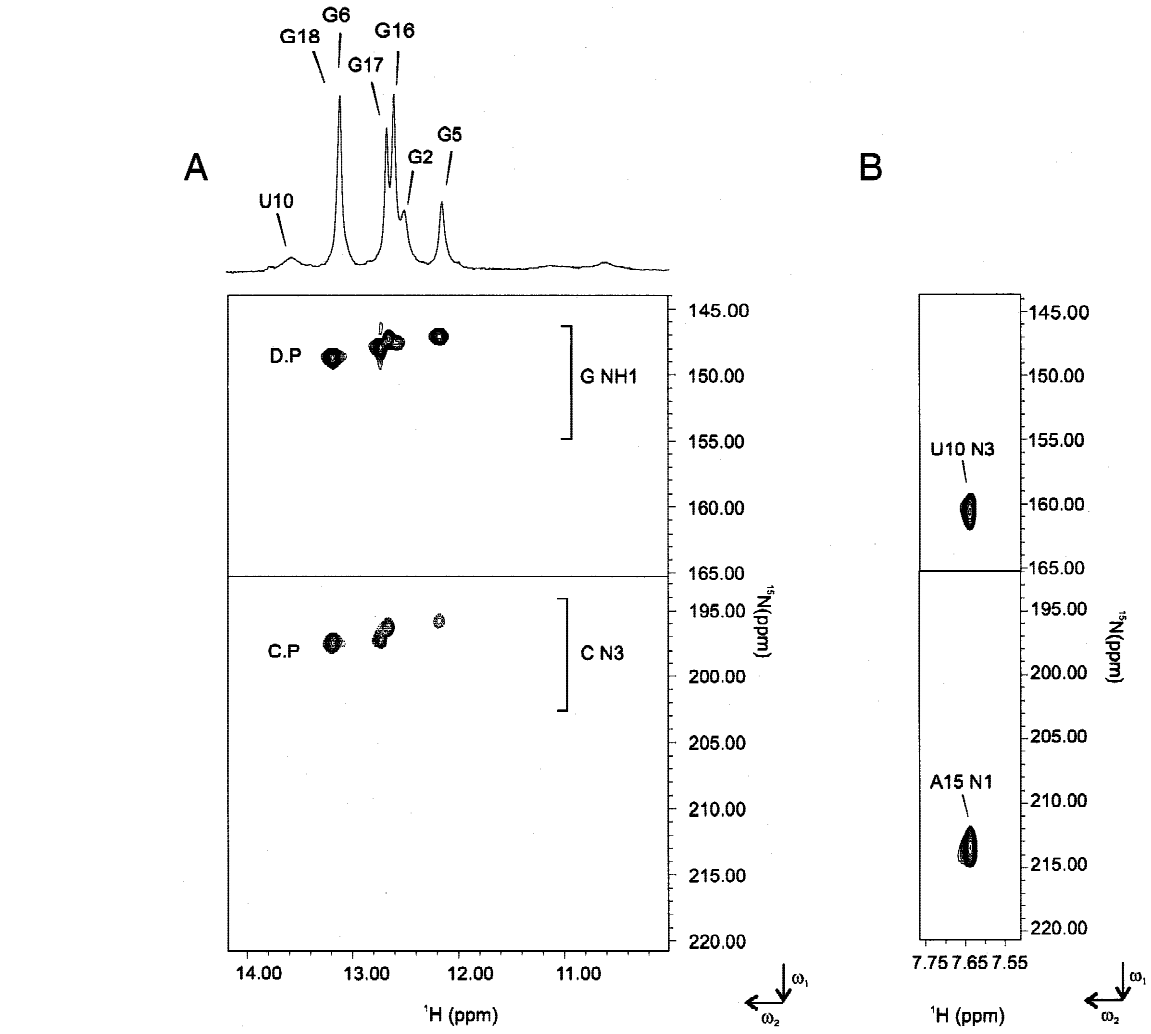

FIGURE 2. **A:** Spectrum of the HNN-COSY experiment showing NN connectivities in CG and GC base pairs in the stem. Shown on top is the imino region of a one-dimensional jump-return spectrum recorded on an unlabeled sample at the same temperature and buffer conditions. **B:** Spectrum of a long-range HNN-COSY experiment optimized for observation of the $^{2h}J_{NN}$ couplings via nonexchangeable protons. The diagonal and cross-peaks for the N1-N3 hydrogen bond in the closing U-A base pair are shown. **C:** Sequential anomeric to aromatic NOE walk from the 300 ms two-dimensional NOESY in D_2O. Solid lines indicate H1′ to H8/H6 connectivities clear in the two-dimensional NOESY spectrum. Red dashed lines highlight steps of the walk established from the three-dimensional HMQC-NOESY spectra. Upper-case letters indicate intraresidue H1′-H6/H8 NOEs, and lower-case letters the strong H5-H6 cross-peaks. Crosses are used to mark missing cross-peaks. **D:** Intraresidue and sequential through-bond correlations for residues 10 to 15. Shown are plots of the C3′ and C4′ planes of the three-dimensional HCP experiment. Intraresidue C(4′)H-P cross-peaks are labeled with upper-case letters. Crosses indicate missing cross-peaks. (*Figure continues on facing page.*)

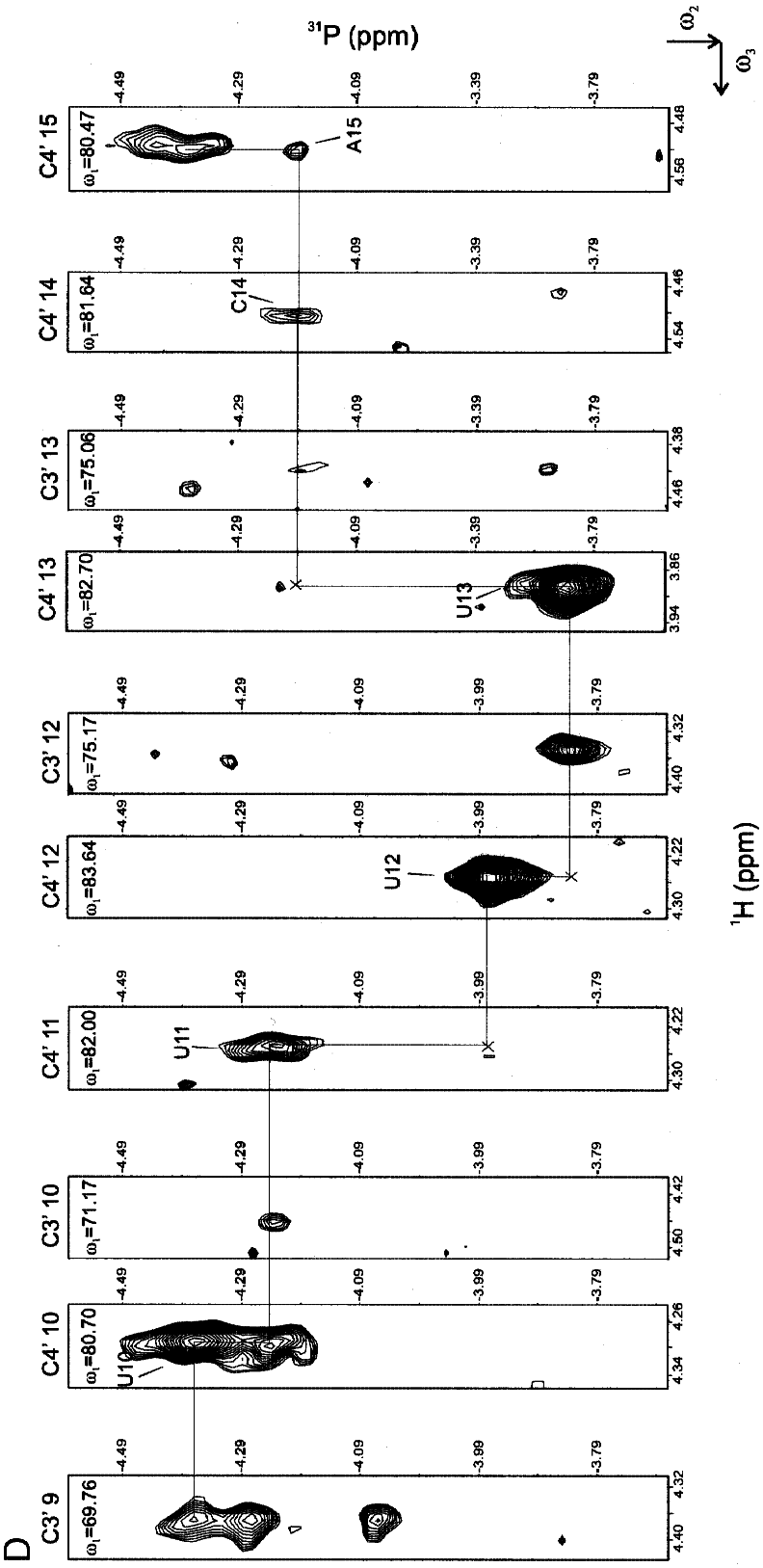

FIGURE 2. *Continued.*

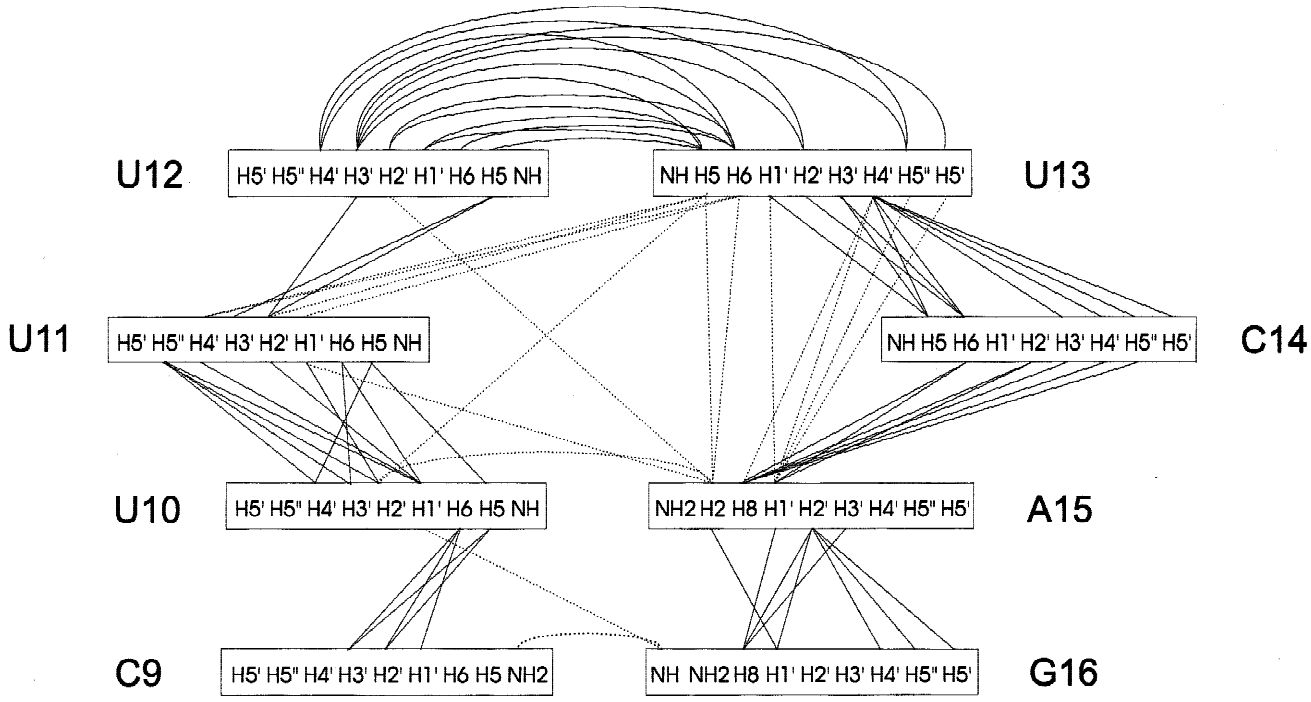

FIGURE 3. Overview of the interresidual NOEs in the histone hairpin loop. Sequential and long-range NOE connectivities are shown by solid and dotted lines, respectively.

Structure of the histone 3′ RNA hairpin

Consistent with the Watson–Crick base pairing scheme, the NOE pattern typical for A-helical RNA terminates at the U10-A15 base pair, and the U11-U12-U13-C14 tetraloop in the 3′ histone mRNA hairpin adopts a well-defined conformation (Figs. 4 and 5). The UUUC tetraloop conformation is stabilized by a combination of stacking and hydrogen bond interactions. A triple base stacking is found at the major groove face of the hairpin loop, involving the closing U10-A15 base pair, U11 and U13. In contrast, the poorly conserved U12 is exposed into the minor groove, and the base of C14 is bulged out towards the minor groove (Figs. 5 and 6).

U13 mediates a large number of interresidual NOE contacts that are important in determining the architecture of the loop (Fig. 3). NOEs between the ribose protons of U13 and the H1′ and H8 protons of A15 define the orientation of the U13 sugar ring (Fig. 5), whereas the base of U13 is positioned by NOE contacts with the sugar protons of U11 and with the base of A15. NOEs between the base of U11 and the sugar of U10 indicate continuation of stacking on the 5′ side of the loop. However, a number of observed sugar/sugar contacts between U10 and U11 (U10 H1′ to U11 H2′, H4′, and H5″) deviate from A-helical stacking and resemble B-helical geometry. The location of U12 in the minor groove is especially supported by a contact between the H2′ of U12 and the H2 of A15, and weak NOEs between the U12 and U13 base protons.

The experimental J-couplings that define the sugar pucker and backbone angles (Table A2 in the Appendix) show that all four loop residues adopt non-A-helical conformations, allowing for the reversal of the phosphodiester backbone. The phosphates of U12, U13, and C14 are flanked by unusual α and ζ torsion angles. For U12 and U13, this is reflected in upfield shifts of the ^{31}P chemical shifts. Whereas the J-couplings measured in the ribose of U11 indicate averaging between C2′ and C3′ endo sugar puckers, the ribose rings of U12 and U13 are shifted to a predominant C2′-endo conformation. The ϵ torsion angles of these nucleotides are gauche$^-$, as expected from known stereochemical correlations between the sugar pucker and ϵ angles (Saenger, 1984). C14 is bulged out from the core of the loop and is not very well defined in the structure ensemble, consistent with a smaller number of NOEs and nonextreme J-coupling values observed for this residue. In 12 out of 15 converged structures, a potential hydrogen bond is observed between the nonbridging phosphate oxygen of U13 and the 2′ hydroxyl of U11 that may stabilize the inversion of the phosphate backbone (Fig. 5C).

In summary, the loop conformation in the histone mRNA hairpin is primarily defined by base stacking interactions and further stabilized by a backbone hy-

TABLE 1. Structural statistics for the histone 3′ hairpin RNA.

Distance restraints[1] (all NOEs)	451
intra ($i = j$)	319
inter ($i \neq j$)	132
residues 5–20 (all)	336
residues 10–15 (all)	118
Hydrogen bonds	23
Torsion angle restraints[2] (all)	158
Backbone (α, β, γ, ϵ, ζ)	80
Sugar pucker (δ, $\phi_{1',2'}$, $\phi_{2',3'}$)	54
Base (χ_1)	24
Rms deviation from experimental restraints	$\langle$SA$\rangle$[3]
Distance restraints (Å)[4]	0.050 ± 0.002
Torsion angle restraints (°)	0.128 ± 0.004
Coordinate precision (Å)[5]	
Residues 10–15	
Backbone	0.53 ± 0.36
Heavy atoms	0.79 ± 0.55
Residues 5–20 (heavy atoms)	0.89 ± 0.29
Number of restraints per nucleotide (residues 5–20)	
Distance restraints	21
Torsion angle restraints	8

[1]Distance restraints were derived from three-dimensional ^{13}C-edited NOESY spectra with 100 and 150 ms mixing times and corrected for spin diffusion by a reduced relaxation matrix approach (J.P. Linge & M. Nilges, in prep.). Distance restraints for the ARIA/CNS calculations were employed with a soft square-well potential (Nilges & O'Donoghue, 1998) using an energy constant of 50 kcal mol^{-1}Å^{-2}. During the AMBER refinement an energy constant of 32 kcal mol^{-1}Å^{-2} was used. The standard AMBER flat-bottom NOE potential was defined with the parabolic region extending to 0.5 Å below/above the lower/upper distance bounds. 1 kcal = 4.18 kJ.

[2]Torsion angle restraints were applied as described in Materials and Methods. Energy constants for the torsion restraints were 5, 25, and 200 kcal mol^{-1} rad^{-2} for the hot, first cooling and second cooling stages in the ARIA/CNS calculations. Torsion angle energy constants in AMBER were 20 kcal mol^{-1} rad^{-2}.

[3]$\langle$SA$\rangle$ is an ensemble of the 15 lowest energy-solution structures of the histone hairpin RNA. Structures were calculated with ARIA/CNS as described in Materials and Methods. The PROLSQ E_{repel} function was used to simulate van der Waals interactions with an energy constant of 25.0 kcal mol^{-1} A^{-4}; Rms deviations for bond lengths, bond angles, and improper torsion angles are 0.0037 ± 0.0001 Å, 0.577 ± 0.011°, and 0.351 ± 0.007°. No distance restraint was violated by more than 0.5 Å in any of the final structures, with the exception of one intraresidual NOE. No torsion angle restraint was violated by more than 2°. Fifteen low-energy structures (out of 100 calculated with ARIA/CNS) were selected for refinement with AMBER using a Generalized Born model for electrostatic interactions. The rms deviations for bond lengths and bond angles for the AMBER calculations are 0.0106 ± 0.0028 Å and 2.46 ± 0.66°, respectively.

[4]Hydrogen bond distance restraints (Saenger, 1984) were applied with error bounds of ±0.1 Å (±0.3 Å for the closing U-A base pair).

[5]Coordinate precision is given as the pairwise Cartesian coordinate rms deviation of the 15 final structures in the AMBER ensemble.

drogen bond. The "core" of the UUUC tetraloop is formed by residues that are conserved in vertebrate histone genes (Fig. 6). The Watson–Crick groups of the U10-A15 closing base pair, and the conserved U11 and U13 loop residues are exposed into the major groove. The functional groups of these conserved nucleotides may thus be utilized for specific RNA recognition by HBP. We therefore tested whether these conserved nucleotides are also important for HBP binding.

HBP binding and thermal stability of RNA mutants

Band shift experiments with hairpin RNA variants

To delineate the individual contributions of residues 10 to 15 for the HBP interaction, we compared the binding of HBP to the H4-12 hairpin RNA (HP) with the binding to hairpins with single or double base substitutions. The hairpins are named according to the base exchanges introduced. For example, in RNA A15G, the adenine at position 15 is replaced by a guanine. The importance of positions 10 and 15 for HBP binding is investigated with three RNAs: A15G, U10A/A15U, and U10C. Whereas in the first two RNAs base-pairing potential is maintained (the A15G mutant may define a potential U-G wobble base pair), U10C is expected to disrupt the closing Watson–Crick base pair of the tetraloop. In additional RNA variants, the pyrimidine bases in the loop between U11 and C14 were changed to U11G, U11C, U12G, U12C, U13C, U13G, C14G, and C14U. The C14U hairpin is found in at least one human histone H4 gene (GenBank Accession X60483) and in a mouse histone H4 gene (V00753), and U12C occurs in human and mouse histone H4 genes (X83548, U62672, Y12290). The other hairpin sequences were not found in vertebrate histone genes in database searches. However, it is possible that some of these loop sequences exist in the context of different stem sequences.

RNA/HBP binding studies were done with recombinant human HBP and ^{32}P-labeled RNAs. In these experiments, the concentration of HBP was 250 nM as determined by Bradford assay. When tested for RNA binding, 250 nM HBP had an RNA binding capacity of 17 ± 2 nM HP RNA (data not shown). This difference between RNA-binding activity and protein concentration may be due to a low reactivity of HBP in the Bradford assay. Alternatively, it may indicate that the HBP preparation is only partially active in RNA binding. All HP RNA was bound in the presence of excess HBP (data not shown). Therefore, to compare the binding behavior of the different hairpin RNAs, we measured the binding of ^{32}P-labeled RNAs to HBP. Binding reactions were analyzed by native gel electrophoresis and detected by autoradiography or using a phosphorimager. The results of the mutational analysis are summarized in Figure 7 and Table 2. Figure 7A shows the binding of the HP and mutant RNAs to HBP under identical conditions. The HP, U12C, U12G, C14U, and C14G RNAs bind with comparable efficiency to HBP (Fig. 7A, lanes 1, 6, 7, 10, and 11), whereas binding of U10A/A15U, U11C, U11G, U13C, U13G, and A15G is strongly reduced (Fig. 7A, lanes 3, 4, 5, 8, 9, and 12). The U10C change has the greatest effect on binding (Fig. 7A, lane 2), and we consistently failed to detect complexes with this RNA in our experiments.

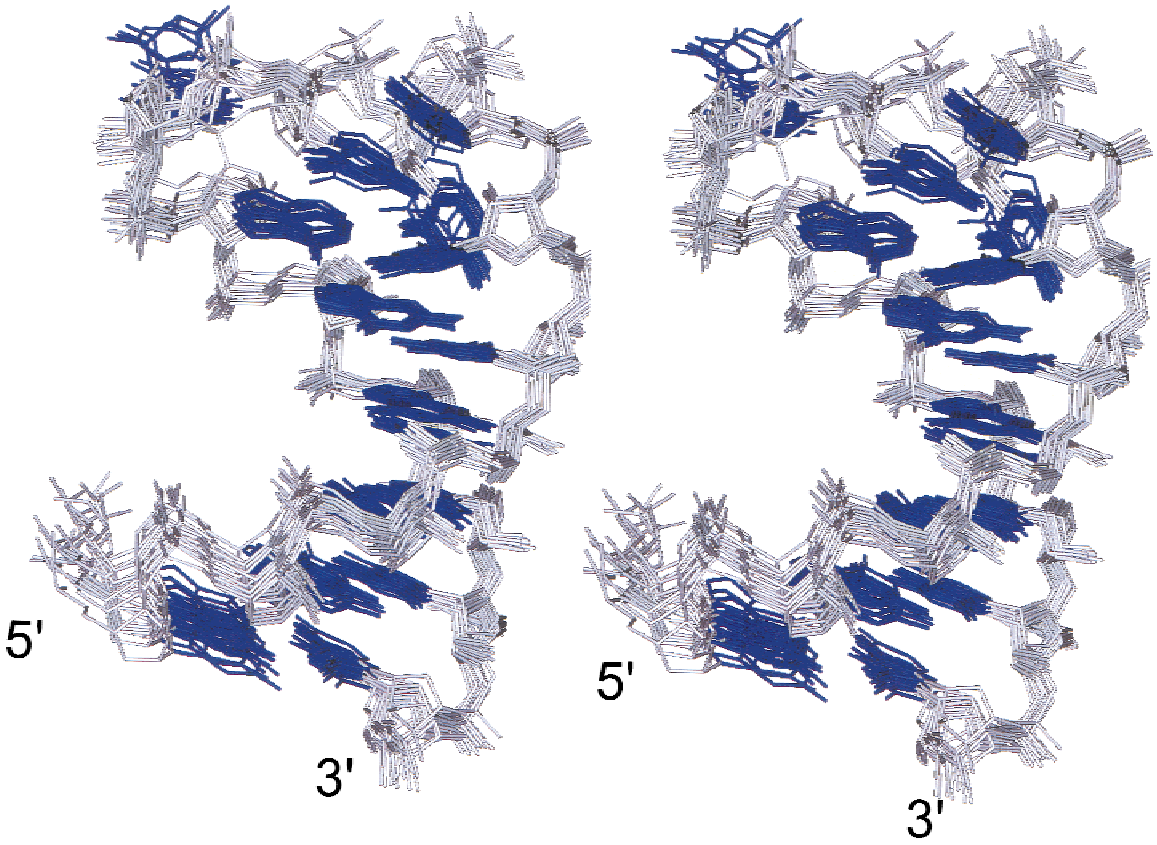

FIGURE 4. Stereo view from the major groove of the final ensemble of the 15 lowest energy structures of the histone mRNA hairpin (residues G5 to C20). Bases are colored in blue and the sugar–phosphate backbone in gray.

To further analyze the differences in binding behavior of these RNAs, we performed a series of binding reactions at constant HBP concentration and varied RNA concentrations. The binding reactions were analyzed by EMSA and the binding efficiency was determined using a Fuji imager. In Figure 7B, the data obtained for HP, C14G, and U10A/A15U RNAs are shown. In reactions with HP RNA, binding increases in a linear fashion up to an RNA concentration of 20 nM, and then reaches a plateau of 14–17 nM RNA bound. This does not change significantly, even after a further increase of the RNA concentration (Fig. 7B and data not shown). In contrast, binding with C14G increases similarly over the whole range of RNA concentrations tested, revealing a difference in affinity not detected in Figure 7A. Binding of U10A/A15U RNA was consistently poor. Dissociation constants (K_d) determined from the data shown in Figure 7B are summarized in Table 2. Wild-type HP RNA, with a K_d of 9 nM, has the highest affinity for HBP of all RNAs tested here. Strong binding is maintained with U12C, and the affinities of U12G, C14U, and C14G are reduced approximately two- to threefold. The strongly reduced HBP interaction observed for U11C, U11G, U13C, U13G, A15G, and U10A/A15U RNAs is

TABLE 2. HBP binding and thermal stability of histone hairpin mutants.

RNA	K_d (nM)	T_m (°C)
HP	9 ± 3	77.3
U10A/A15U	>40	77.8
U10C	No binding	73.0
U11C	>40	—
U11G	>40	n.d.
U12C	11 ± 4	—
U12G	20 ± 7	—
U13C	>40	77.7
U13G	>40	77.4
C14U	29 ± 10	—
C14G	26 ± 8	—
A15G	>40	77.1

Effects on affinity to HBP and thermal stability of the RNA mutants. Mean and standard deviation values of the dissociation constants (K_d) have been derived from at least four independent experiments. A $K_d > 40$ was assigned when binding was observed, but signals were too weak to be quantitated reliably. Melting temperatures (T_m) are shown for a H2A 16-mer RNA containing loop mutations that severely reduce HBP binding (i.e., with a $K_d > 40$ nM). The normalized melting profiles of all constructs tested, with the exception of the U11G mutant, are characterized by a single transition and are concentration independent over a 20-fold range (data not shown). The melting profile of the U11G mutant was not interpretable due to multiple transitions (n.d.).

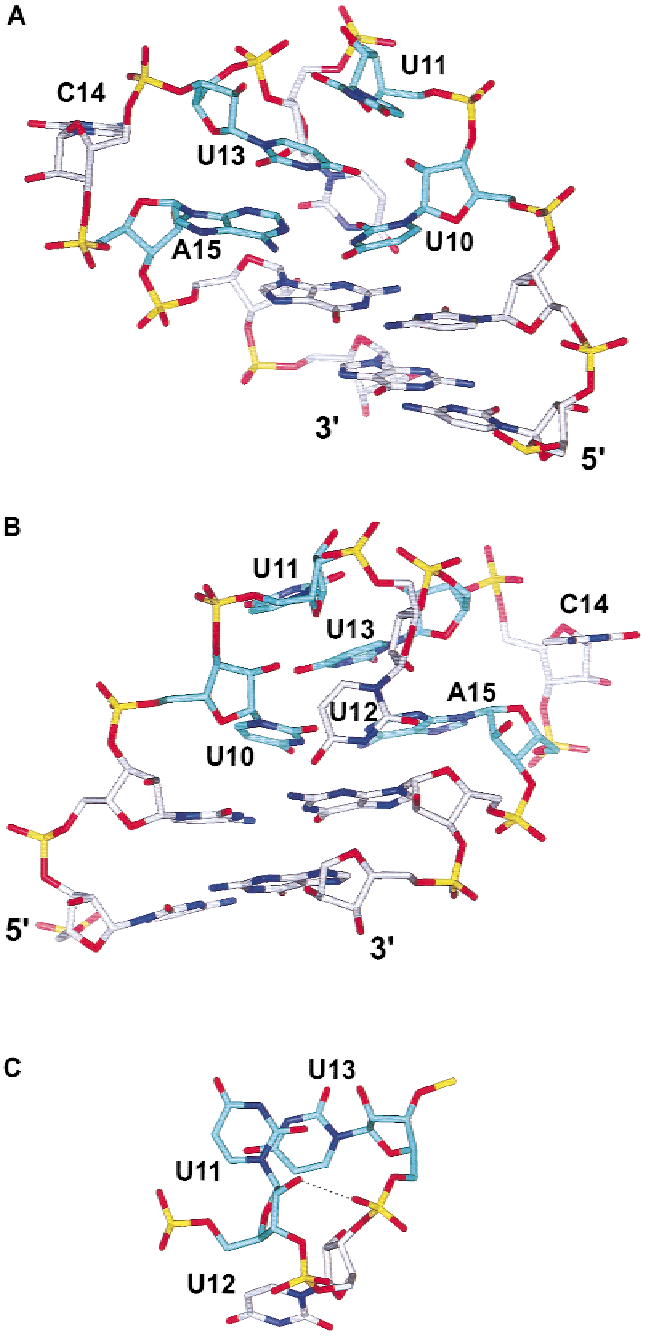

FIGURE 5. Minor (**A**) and major (**B**) groove views of the lowest energy structure of the hairpin loop (residues C8 to G17). The conserved loop residues (U10, U11, U13, and A15) are colored in cyan. **C:** A view rotated by ~90° around the x-axis compared to **B** showing U11, U12, and U13 . Base stacking and potential hydrogen bonding (dotted line) between residues U11 and U13 are visible.

confirmed. For these RNAs, HBP binding is detectable but the data obtained did not allow for accurate calculation of the dissociation constant.

A comparison of these results with the histone hairpin sequence in Figure 7C reveals that exchanges of the highly conserved hairpin residues U10, U11, U13, and A15 have a severe effect on the ability of the RNA

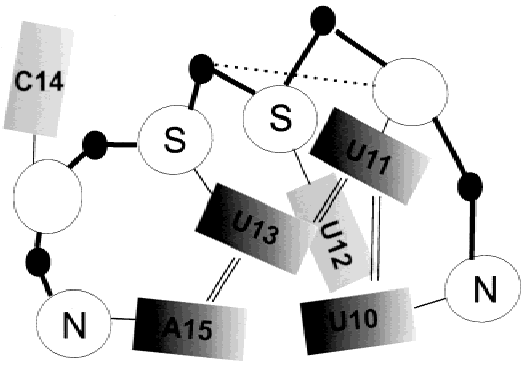

FIGURE 6. Schematic overview of the hairpin loop. Symbols are ellipses (sugars), rectangles (bases), filled circles (phosphates). Stacking interactions and hydrogen bonds are shown with double and dashed lines, respectively. Sugar puckers defined by the experimental J-couplings are indicated.

to bind to HBP. As described above, these residues form the core of the loop structure and have their Watson–Crick functional groups oriented towards the major groove. In contrast, changing the nonconserved residues U12 and C14 has only a small effect on HBP binding.

Thermal stability of hairpin mutants

The thermal stabilities of the RNA hairpin and variants that had a large effect on HBP binding were characterized based on their melting points (Table 2). The loop mutations were introduced in a H2A 16-mer hairpin construct (Battle & Doudna, 2001) that differs from that of the histone H4 hairpin shown in Figure 1 only in the fourth stem-base pair (Table 2; see Materials and Methods). The lower thermal stability conferred by this U-A base pair in the H2A 16-mer construct allows observation of the full melting transition.

The 16-mer hairpin with the wild-type UUUC loop sequence has a rather high melting temperature ($T_m = 77\,^{\circ}C$). Assuming a two-state helix-coil transition, an approximate value for the enthalpy of melting, $\Delta H(T_m) = -67 \pm 4$ kcal mol^{-1} can be obtained using the relation $\Delta H(T_m) = -4RT_m^2/\Delta T_{1/2}$ where $\Delta T_{1/2}$ is the width of the transition and R the universal gas constant (Riesner et al., 1973). The nearest neighbor model (Freier et al., 1986) predicts $\Delta H(T_m) = -55$ kcal mol^{-1} for the stem of the 16-mer RNA. Thus, the difference of 12 kcal mol^{-1} indicates that the tetraloop contributes an additional enthalphy comparable to the cost of extending the hairpin by an additional base pair.

The loop variants U13C, U13G, A15G, and U10A/A15U have melting profiles very similar to the wild-type construct, with a T_m of 77 °C, suggesting that these mutations do not destabilize the hairpin conformation. The lower melting point ($T_m = 73\,^{\circ}C$) of U10C suggests that this base exchange affects the stability and pre-

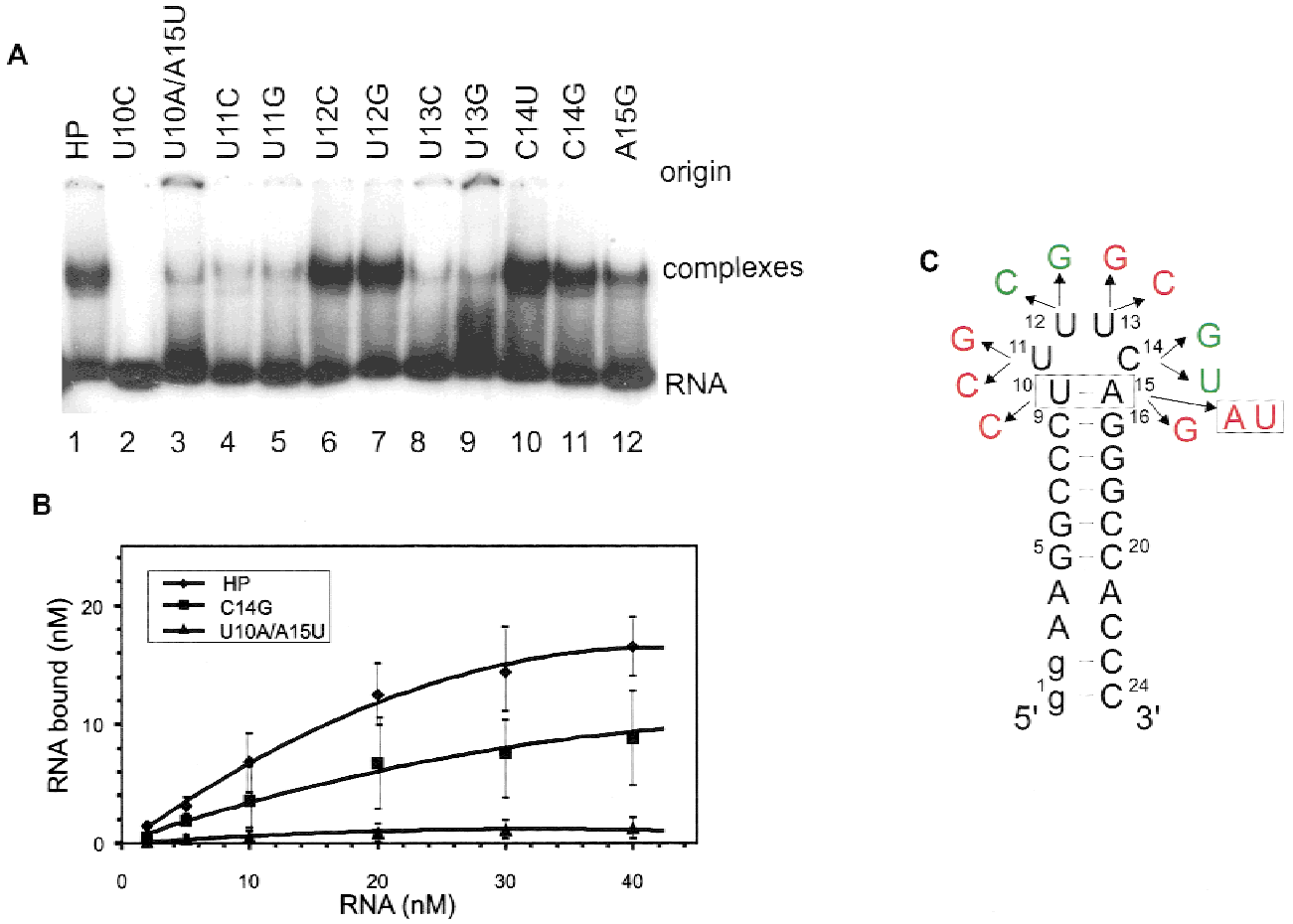

FIGURE 7. Binding of HBP to hairpin RNAs. **A:** Analysis of binding reactions by EMSA. Binding reactions with 10 nM RNA and 250 nM recombinant HBP were done as described in Materials and Methods, analyzed by EMSA, and visualized by autoradiography. RNAs used are indicated at the top. **B:** Graph summarizing binding reactions done with wild-type (HP), C14G, and U10A/A15U RNA. Binding reactions were done with 250 nM HBP and with RNA between 2–40 nM and were analyzed as in **A**, visualized by phosphorimager, and the concentration of RNA in HBP-RNA complexes was determined. The graph shows the mean and standard deviations of RNA bound (in nanomolar) at the indicated RNA concentrations. **C:** Conserved residues in the histone hairpin loop are important for RNA/HBP interaction. Summary of the effects of base substitutions on HBP binding. Effects are divided into weak (green) and strong (red, >4-fold reduction).

sumably structure of the hairpin, that is, by eliminating the closing base pair.

DISCUSSION

Conformation of the UUUC tetraloop

The structure of the UUUC tetraloop in the histone mRNA hairpin differs from other known classes of hairpin loops, that is, UNCG, GNRA, and CUUG (N is any nucleotide and R is a purine; Moore, 1999; Gutell et al., 2000), mainly in the absence of base pair formation between the first and last nucleotides in the sequence. In contrast to these motifs, which are in fact biloops, the UUUC sequence is a true tetraloop. The UUUC loop conformation is also distinct from classical U-turn motifs (consensus sequence UNRN) such as the anticodon loops in tRNA molecules, as the characteristic base stacking and hydrogen bond interactions with loop phosphates are not observed.

Some of the NOE contacts between U11 and U12 and between U11 and U13 are reminiscent of those observed between the first two residues (U5 and U6) and the first and the third residue (U5 and C7) in the UUCG tetraloop (Cheong et al., 1990; Allain & Varani, 1995). In addition, in both the UUCG and the CUYG (Jucker & Pardi, 1995) loops, the nucleotide in the second loop position is located in the minor groove side of the loop, whereas the third loop nucleotide is exposed into the major groove. A comparable topology is found in the UUUC loop reported here, where U12 and U13 are oriented towards the minor and major grooves, respectively. In contrast to the additional loop base pairs between the first and fourth loop residue in the CUYG, UUCG, and GNRA biloops, and distinct from the long-range base-phosphate hydrogen bond and stacking interactions found in U-turns, the UUUC loop is primarily stabilized by base–base stacking and a sugar–phosphate hydrogen bond involving the first and third loop residues.

The hairpin structure presented here is similar to that reported in the accompanying article (DeJong et al., 2002). Both structures exhibit a UUUC tetra-loop conformation that is primarily stabilized by stacking interactions involving the conserved first and third loop uridines (U11 and U13 in this study). In both structures, the loop cytosine (C14) is less well defined and oriented away from the core of the loop. The two structures differ with respect to the conformation of the nonconserved second loop uridine (U12), which in the present study is located in the minor groove, whereas it stacks onto the first loop uridine in the structure reported by DeJong et al (2002). The differences likely result from the buffer conditions used (10 mM Na^+, pH 6.0 versus 40 mM K^+, pH 6.8), and are reflected in distinct experimental observations. For example, the loop uridine imino protons are somewhat protected against solvent exchange in the structure reported by DeJong et al. (2002), whereas they are solvent exposed in the structure presented here, consistent with the imino spectra (Fig. 2 in both articles). The structural differences are manifested in distinct NOE patterns. NOEs that define the triple base stacking and the location of the U12 in the minor groove in this study are not observed in the study of DeJong et al. (2002). The observed differences indicate structural variability for U12 that might also be present at physiological conditions. However, this is unlikely to be important for the biological function of the hairpin RNA, because both conformations are very similar with respect to the highly conserved, functional important residues that are located in the major groove (see below).

Sequence- and structure-specific RNA recognition by HBP

The binding data presented here complement a series of in vitro and in vivo studies on the HBP RNA interaction (Dominski et al., 1999; Martin et al., 2000; Michel et al., 2000; Battle & Doudna, 2001). The K_d value for the wild-type RNA HBP complex (9.0 $\pm$ 3 nM) demonstrates formation of a stable protein–RNA complex. In a recent report (Battle & Doudna, 2001), slightly higher binding affinities of 0.85 to 1.5 nM were described for human and *Xenopus* HBPs in complex with wild-type hairpin RNA from the mouse H2A histone gene. The differences in the K_d values are likely attributable to the RNA constructs used, particularly to differences in the 5′ and 3′ flanking regions. Approximately threefold lower K_d values were also reported for the interaction between HBP RNA-binding domains (HBP RBD) and hairpin RNAs (Michel et al., 2000). Analysis of our new and the previously described data reveals a strong correlation between the importance of nucleotides for the HBP interaction and the conservation of residues in the hairpin RNA sequence (Fig. 7): U10, U11, U13, and A15 are all highly conserved and exchange of these residues leads to a strong reduction in RNA binding.

Recognition of the closing U10-A15 base pair

The UV melting data (Table 2) show that inversion of the closing base pair (U10A/A15U) does not significantly affect hairpin stability. This is consistent with the structure of the hairpin, as the bases of 10 and 15 are only involved in non-sequence-specific stacking interactions with other loop residues. Thus, base pair inversion should not destabilize the loop conformation. However, the U10A/A15U mutation strongly reduces the protein–RNA interaction indicating that HBP discriminates between U10-A15 and a reverse A10-U15 base pair. This is expected if RNA recognition occurs in the major groove side of the stem (Seeman et al., 1976). No change in hairpin stability is seen for the A15G mutant that might be explained by the formation of a closing U-G base pair. Hence, the reduced HBP interaction of the A15G mutant could result from substitution of the exocyclic A15 N6 by a keto group. The U10C mutation eliminates HBP binding completely. This presumably results from the loss of the closing base pair (as suggested by the 4 °C lower melting point of the U10C mutant). Taken together, the structural and mutational data suggest that HBP recognizes the major groove side of the closing U10-A15 base pair of the tetraloop and show that this base pair is crucial for HBP binding.

Recognition of U11 and U13

The thermal stability of both U13C and U13G mutants is comparable to the wild-type RNA suggesting that the fold of the hairpin is not affected by these mutations. This is also expected from the structure of the hairpin RNA, as the Watson–Crick functional groups of U13 are solvent exposed and not involved in RNA–RNA contacts. The strong reduction of HBP binding to the U13C RNA thus indicates that the Watson–Crick functional groups of U13 are required for the specific recognition by HBP.

The U11C and U11G hairpin mutants interact with HBP only weakly. A significant reduction in RNA binding with U11C RNA (in a *C. elegans* hairpin sequence context referred to as ceHP-CUUC loop RNA) was also observed in experiments with the human HBP RBD (Michel et al., 2000). This is further supported by the observation that the identity of the pyrimidine base at position 11 is the main determinant enabling the *C. elegans* HBP to discriminate between human UUUC and *C. elegans* CUUU hairpin loops (Michel et al., 2000; Dominski et al., 2001). Taken together, these data show that U11 significantly contributes to HBP binding, and that the Watson–Crick face of U11 is specifically recognized.

In contrast to the effect of mutations at positions 10, 11, 13, and 15, changes of the poorly conserved bases

at positions 12 and 14 have no or only small effects on HBP binding (Fig. 7; Table 2). This is supported by the structure of the hairpin, as the U10, U11, U13, and A15 bases that are important for HBP binding are facing the major groove of the hairpin structure whereas both the U12 and C14 bases are oriented away from the major groove.

Consistent with the results described here, previous mutational studies have shown that base changes at positions 11, 13, and 15 lead to reduced affinity for HBP (Pandey et al., 1994; Martin et al., 2000; Battle & Doudna, 2001). Using the yeast three-hybrid system to measure protein–RNA interactions, it was found that the loop mutants U11G and U13A as well as the double mutant U11G/U13A led to a significant decrease in marker gene activation (Martin et al., 2000). Although it is not possible to precisely measure affinities in this system, this finding is in agreement with our observation that the conserved loop residues are important for RNA binding. In a recent study (Battle & Doudna, 2001) using filter binding assays, it was found that single-, double-, and triple-base replacements of nucleotides between positions 11 and 14 drastically reduce the affinity for HBP. The single base changes tested complement those described in Figure 7 and Table 2. L-UUAC and L-AUUC RNAs that correspond to RNAs U13A and U11A led to a 17- to 22-fold reduced affinity for HBP. SL-UG6 RNA, corresponding to A15G, caused a similar reduction for HBP binding. These observations are in agreement with the decrease in affinity observed for U11C, U11G, U13C, U13G, and A15G RNAs described herein.

Previously, it was shown that hairpin RNA/HBP binding correlates with efficient pre-mRNA processing. Marzluff and coworkers found that base substitutions of residues 10, 11, 13, and 15 that severely affect the HBP interaction also lead to 80 to 95% reductions of in vivo histone pre-mRNA processing (Pandey et al., 1994). This shows that the same nucleotides that are crucial for HBP binding are also required for the functional activity of the 3′ hairpin in vivo.

A model for the histone 3′ hairpin/HBP complex

The minimal RNA-binding region of HBP is predicted to form three α-helices. Michel et al. (2000) have identified two amino acid sequence elements in the RBD (YGKNT between helix 1 and 2 and FKKY between helix 2 and 3, respectively) that are involved in RNA binding and sense the base at position 11. The combined analysis of the hairpin structure and the mutational data reveals that HBP binding requires the sequence-specific recognition of U10, U11, U13, and A15 in the major groove side of the tetraloop. The recognition of the nucleotide at position 11 by two amino acid stretches in short loops interspersed between helices suggests that one of these helices may bind into the major groove whereas the "specificity" loops may contact the base at position 11.

In addition, inversion of the first and second G-C stem base pairs (G5-C20 and G6-C19) and deletion of nucleotides flanking the 5′ and 3′ ends of the hairpin (Martin et al., 2000; Battle & Doudna, 2001) also reduce HBP binding. This indicates that the lower part of the hairpin structure is also recognized by HBP, presumably involving additional regions in the protein.

The predicted α-helical structure of the HBP RBD and the major groove recognition of the RNA hairpin is reminiscent of DNA binding by the helix-turn-helix motif that is found in a large family of DNA-binding proteins (Luscombe et al., 2001). DNA recognition by the helix-turn-helix motif occurs via insertion of a recognition helix into the major groove of B-form DNA. The narrower major groove in A-form RNA helices does not allow insertion of a protein α-helix. However, widening of the major groove near the hairpin loop and at the bottom of the hairpin stem may allow amino acid side chains to protrude into the major groove and mediate hydrogen bonds with the Watson–Crick functional groups for sequence-specific recognition of the hairpin RNA.

CONCLUSIONS

The three-dimensional structure of the histone 3′ RNA hairpin reveals a compact UUUC tetraloop conformation that is stabilized by a triple stacking interaction of the first and third loop residues with the closing U-A base pair. The phosphodiester backbone turn is stabilized by a sugar–phosphate hydrogen bond involving the first (U11) and third (U13) residues in the tetraloop. The stacking and hydrogen bonding interactions may explain the stability of the hairpin element observed in temperature denaturation experiments.

The analysis of the tetraloop structure and the HBP interaction of wild-type and variant hairpin RNAs reveals a strong correlation between evolutionary conserved residues and their importance for the loop conformation, HBP binding, and function in histone RNA processing. The architecture of the UUUC tetraloop exposes the Watson–Crick functional groups of evolutionary conserved nucleotides into the major groove of the RNA hairpin. Crucial interactions for HBP recognition are mediated by these residues, in particular by the closing U10-A15 base pair and the first and third loop nucleotides (U11 and U13). Our results provide novel structural insight into the interaction of the histone 3′ hairpin with HBP, and thus the regulation of histone mRNA metabolism.

MATERIALS AND METHODS

RNA synthesis and purification

Unlabeled, ^{15}N- and ^{15}N, ^{13}C-labeled RNA samples were prepared by in vitro transcription of a synthetic DNA template

using phage T7 RNA polymerase (Milligan et al., 1987). Nucleotide triphosphate precursors for the synthesis of the labeled samples were obtained from bacterial sources according to already published methods (Price et al., 1998). Purification was performed using denaturing polyacrylamide gel electrophoresis and electroelution. The purified RNA transcript was first ethanol precipitated and then subjected to step-dialysis against phosphate buffer at pH 6.0 with progressively decreasing salt concentrations (from 1 to 0 M NaCl; G. Varani, pers. comm.). The RNA was desalted using a Sephadex G-25M column (Amersham Pharmacia Biotech) and subsequently lyophilized. The molecular weight of the RNA transcript was confirmed by mass spectroscopy.

NMR experiments

NMR sample buffer conditions were 10 mM sodium phosphate, pH 6.0, 0.1 mM EDTA, 10% D_2O or 100% D_2O with RNA concentrations of 1.0 mM. NMR samples were annealed prior to NMR experiments by heating at 100 °C for 10 min and snap cooling on ice for 10 min to ensure homogenous formation of monomeric hairpin conformation. NMR data were acquired at either 12 °C or 25 °C on Bruker DRX500, DRX600, or DRX800 spectrometers.

To distinguish between monomeric and dimeric RNA conformations under NMR sample conditions we developed a novel NMR-based method which is based on the measurement of $^{2h}J_{NN}$ coupling constants across hydrogen bonds in the Watson–Crick base pairs of the RNA (K. Zanier & M. Sattler, in prep.). We found that the relative intensity of cross-peaks and diagonal peaks in HNN-COSY experiments (Dingley & Grzesiek, 1998) recorded on a 50% ^{15}N-labeled/50% unlabeled sample is comparable to what is observed for a 100% ^{15}N-labeled sample (data not shown). This is expected for intramolecular base pairs and thus for a monomeric hairpin conformation. In a homonuclear TOCSY spectrum, the correct number of H5-H6 cross-peaks expected for the 13 pyrimidine bases of the hairpin was observed. The chemical shifts of the loop base protons are largely independent of temperature, ruling out large conformational changes between 5 and 45 °C. Taken together, these data indicate that the 24-mer RNA adopts a homogenous monomeric hairpin conformation.

Hydrogen bonds across Watson–Crick base pairs were measured in $^{2h}J_{NN}$ HNN-COSY experiments (Dingley & Grzesiek, 1998; Hennig & Williamson, 2000; Luy & Marino, 2000) to establish the base-pairing scheme in the stem region. NMR experiments correlating cytosine H5 protons to cytosine N3 and the N1 of base-paired guanosines (not shown) were used to independently confirm sequential assignments for the C-G base pairs. Five hydrogen bonds are detected for C-G base pairs (Fig. 2A). The G1 imino resonance is not observed, and no cross-peak is detected for the G2-C23 base pair in the HNN-COSY experiment, presumably due to end fraying of the stem. Exchangeable protons and ^{15}N chemical shifts were assigned in two-dimensional WATERGATE or jump-return NOESY (mixing times: 50, 150, 250, and 300 ms) and ^{1}H,^{15}N-HSQC experiments (Varani et al., 1996; Sattler et al., 1999). Constant-time HSQC, three-dimensional HCCH-TOCSY, and three-dimensional HCCH-COSY (Pardi & Nikonowicz, 1992) were used for sugar assignments. Intranucleotide H1′ to H6/H8 and intrabase correlations were obtained from two-dimensional HCN experiments (Sklenar et al., 1998; Fiala et al., 2000). Aromatic and imino protons in guanine bases were connected in two-dimensional HCCNH-TOCSY experiments (Sklenar et al., 1996). Correlation of adenine H8 and H2 protons was obtained as described (Simon et al., 2001). ^{1}H,^{31}P HETCOR (Kellogg, 1992) and three-dimensional HCP (Heus et al., 1994; Marino et al., 1995) experiments were used to confirm sequential backbone assignments. No sequential connectivities are observed between the H3′ or H4′ protons of U11 and the phosphorus of U12, and only a weak correlation is found between the U13 H3′ and the phosphorus of C14, consistent with unusual α, ζ backbone angles that are found in the structure for this phosphate (Table A2 in the Appendix). Three-dimensional ^{13}C-edited HMQC-NOESY spectra with mixing times of 50, 100, and 150 ms were used for sequential assignment via sugar–base contacts. Two-dimensional NOESY experiments in D_2O (mixing times of 50, 100, 200, 300, and 500 ms) were used to confirm nonexchangeable proton assignments.

Homonuclear ^{1}H,^{1}H J-couplings for the sugar spin systems were measured in DQF-COSY, three-dimensional HCCH-E.COSY (Marino et al., 1996; Zimmer et al., 1996) and three-dimensional forward-directed HCC-TOCSY-CCH-E.COSY (Schwalbe et al., 1995) experiments. A two-dimensional spin echo difference CT-HSQC experiment was used to determine $^{3}J_{C2'P}$ coupling constants (Legault et al., 1995). Data were processed using NMRPipe (Delaglio et al., 1995) and analyzed with XEASY (Bartels et al., 1995).

Structure calculation and refinement

NOEs were manually assigned. The automated NOE assignment and recalibration options of ARIA were not used. Distance restraints were derived from three-dimensional ^{13}C-edited NOESY spectra with mixing times of 100 and 150 ms. The distance calibrations by ARIA included a spin diffusion correction (J.P. Linge & M. Nilges, in prep.) and were manually cross-checked against NOE intensities. Energy constants for distance restraints were 10 and 50 kcal mol^{-1} during the high temperature dynamics and the cooling phases, respectively. NOE contacts observed in NOESY spectra recorded in H_2O were not used during the structure calculations. However these distance restraints were satisfied in the structure.

A-form torsion angle restraints were applied for backbone angles in the stem region. Otherwise, torsion angle restraints were generated from experimentally determined J-couplings only if the data did not indicate conformational averaging (Varani et al., 1996; Wijmenga & van Buuren, 1998). Sugar puckers for C2′-endo or C3′-endo conformations were defined by restraining the torsion angle δ to 140° ± 50° or 82° ± 30°, $\phi_{1',2'}$ to 160° ± 20° or 99° ± 20°, and $\phi_{2',3'}$ to −25° ± 20° or 38° ± 20°, respectively. Restraints for the torsion angle γ of 60° ± 30° were applied if the g^+ conformations was defined based on $^{3}J_{H4'H5'/H5''}$ and $^{3}J_{C4'H5'/H5''}$ coupling constants (Marino et al., 1996). Where J-coupling data were available, the backbone angle ϵ was restrained to either 260 ± 40° (g^-) or to −135 ± 60° (t/g^-, excluding the unfavorable g^+ conformation). The glycosidic χ angles were weakly restrained to the *anti* conformation (190° ± 100°) consistent with the NOE data.

Low energy structures were initially generated starting from a random RNA template using CNS in the ARIA setup (Linge et al., 2001). The standard CNS *dna-rna-allatom.param* force

field was used (Stallings & Moore, 1997) with uniform energy constants for all bond, angle, and improper dihedral energy terms. The protein-specific parts of the calibration and simulated annealing protocols were adopted for nucleic acids. Structures were calculated in two iterations. During the first iteration, hydrogen bond and NOE distance restraints were applied for the Watson–Crick base pairs (energy constant 50 kcal mol^{-1}). Weak planarity restraints (25 kcal mol^{-1} for the C-G base pairs and 5 kcal mol^{-1} for the closing U-A base pair) were applied together with the hydrogen bond restraints. For each hydrogen bond, planarity is defined for a plane that involves one atom of the acceptor and four atoms of the donor base to allow for propeller twist and tilt. Hydrogen bond, planarity, torsion angle, and distance restraints were simultaneously applied during the second iterations. The simulated annealing protocol in CNS consisted of four stages: a high-temperature torsion angle simulated annealing phase (8,900 steps at 10,000 K with a time step of 27 fs), a first torsion angle dynamics cooling stage from 10,000 K to 2,000 K (8,900 steps), a Cartesian dynamics cooling phase from 2,000 K to 1,000 K (80,000 steps), and a Cartesian dynamics cooling phase from 1,000 K to 0 K (32,000 steps) with a time step of 3 fs.

The 15 lowest energy structures resulting from the second iteration (out of 100 calculated) were subjected to restrained molecular dynamics with the SANDER module of the AMBER 6 package (Case et al., 1999) using the Generalized Born implicit solvation model (Tsui & Case, 2000). Hydrogen bond distance, torsion angle, and NOE-derived distance restraints were employed as in the CNS/ARIA calculations. The protocol involved a 20 ps restrained molecular dynamics run, with heating from 0 to 600 K during the first 5 ps, followed by a first cooling step to 100 K (13 ps) and a final cooling step to 0 K (3 ps).

Structures were checked for close proton–proton distances that are inconsistent with the NOESY data. The final ensemble of NMR structures was validated against the experimental NOE-derived distance restraints.

HBP expression and purification

Recombinant human HBP with an N-terminal $M(H)_6LEA$ tag was produced by infection of SF21 insect cells with recombinant baculovirus and purified by Ni-NTA affinity column chromatography as described (Martin et al., 2000). HBP was stored in 20 mM HEPES-KOH, pH 7.9, 20% glycerol, 1 mM EDTA, 100 mM KCl or NaCl, 1 mM PMSF, and 1 mM DTT. The protein concentration (1 mg/mL) was determined using the Bradford assay (Biorad) with bovine serum albumin as reference protein. The RNA-binding capacity of the HBP preparation at a concentration of HBP of 250 nM protein was 17 $\pm$ 2 nM, as determined in binding assays with HP RNA as described below with up to 50 nM HP RNA.

RNA synthesis for binding studies

^{32}P-labeled RNA molecules were produced by transcription of partially double-stranded templates using T7 RNA polymerase as previously described (Michel et al., 2000). The sequence of wild-type hairpin RNA HP (GGAAGGCCCUU UUCAGGGCCACCC) is as in Figure 1. In addition, a series of RNA variants with single or double base substitutions were produced. The nomenclature for these RNAs is based on the structure and numbering shown in Figure 1, and base substitutions are indicated as follows: U10C—substitution of U10 by C. The following variants were produced: U10C, U11C, U11G, U12C, U12G, U13C, U13G, C14U, C14G, A15G, and U10A/A15U. To determine the yield of RNA synthesis and purification, the fraction UTP incorporated was determined and used to calculate the amount of RNA prepared, taking into account the number of uridine residues in the product.

Binding assays

RNA binding assays were performed in 10 mM Tris-HCl, pH 7.5, 10% glycerol, 20 mM KCl, 1 mM DTT, and 1 U/μL RNasin (Promega) in a final volume of 10 μL. Protein concentration was at 250 nM as determined by Bradford assay and ^{32}P-labeled RNA was between 2 and 50 nM. Incubations were on ice for 30 min, followed by analysis by native 5% polyacrylamide gel electrophoresis (Schaller et al., 1997). The result was then visualized and quantified using a Fuji Phosphorimager. When KCl was replaced by NaCl in the HBP storage buffer as well as in the binding reaction, the relative affinities of the RNAs for HBP were similar (data not shown).

Determination of binding constants

Dissociation constants were calculated separately for each experiment using the Scatchard transformation of the binding data. At least four independent determinations were done, and the K_d average and standard deviation for each RNA is shown in Table 2. Binding of HBP to U10A/A15U, U11C, U12G, U13C, U13G, and A15G was very low and we were not able to use the data for a reliable determination of K_d. The K_d for these RNAs is therefore given as $>$40 nM. No binding was observed with U10C.

UV melting experiments

UV absorbance melting profiles at 260 nm were obtained using a CARY UV/VIS spectrophotometer (Varian) equipped with a temperature-controlled heating unit. The heating rate was 0.5 °C. The melting profiles were reversible (i.e., when cooling from 95 to 20 °C). At least five independent measurements were recorded on each RNA sample, with concentrations varying over a 20-fold range (0.5–10 μM) in 50 mM sodium phosphate, pH 7.4. The T_m values were estimated from the maximum in the derivative of the melting curve.

The sequence of 16-mer RNA construct used in these experiments (GGCUCUUUUCAGAGCC) is derived from the mouse H2A histone gene (Battle & Doudna, 2001). The loop mutations introduced in the H2A 16-mer RNA and tested correspond to the U10C, U11G, U13C, U13G, A15G, and U10A/A15U variants of the 24mer RNA construct used in the binding studies.

Accession number

The atomic coordinates of the ensemble of NMR structures for the RNA hairpin have been deposited in the PDB under accession code 1KKS.

ACKNOWLEDGMENTS

We are grateful to Raik Grünberg for advice and support with the AMBER refinement, Bernd Simon for help with NMR experiments, Gabriele Varani for practical advice with RNA sample preparation, Vladimir Sklenar for an HCN pulse program, Wolfgang Bermel (Bruker) for spectrometer time, Brian Sproat (RNA-TEC) for useful discussions, and Hongyuan Mao and Vickie Tsui for advice with AMBER. We thank Eric DeJong and Ed Nikonowicz for mentioning their independent parallel work prior to publication. Support from the European Molecular Biology Laboratory and the Deutsche Forschungsgemeinschaft (M.S.), Fonds voor Wetenschappelijk Onderzoek-Vlaanderen and European Molecular Biology Organisation (I.L.), the Royal Society and the Wellcome Trust (B.M.), and the Boehringer Ingelheim Fonds (J.P.L.) is acknowledged.

Received August 23, 2001; returned for revision September 18, 2001; revised manuscript received October 22, 2001

REFERENCES

Allain FH, Varani G. 1995. Structure of the P1 helix from group I self-splicing introns. *J Mol Biol 250*:333–353.

Bartels C, Xia T-H, Billeter M, Güntert P, Wüthrich K. 1995. The program XEASY for computer-supported NMR spectral analysis of biological macromolecules. *J Biomol NMR 5*:1–10.

Battle DJ, Doudna JA. 2001. The stem-loop binding protein forms a highly stable and specific complex with the 3′ stem-loop of histone mRNAs. *RNA 7*:123–132.

Birchmeier C, Folk W, Birnstiel ML. 1983. The terminal RNA stem-loop structure and 80 bp of spacer DNA are required for the formation of 3′ termini of sea urchin H2A mRNA. *Cell 35*:433–440.

Bond UM, Yario TA, Steitz JA. 1991. Multiple processing-defective mutations in a mammalian histone pre-mRNA are suppressed by compensatory changes in U7 RNA both in vivo and in vitro. *Genes & Dev 5*:1709–1722.

Case DA, Pearlman DA, Caldwell JC III, Cheatham TE, Ross WS, Simmerling CL, Darden TA, Merz KM, Stanton RV, Cheng AL, Vincent JJ, Crowley M, Tsui V, Radmer RJ, Duan Y, Pitera J, Massova I, Seibel GL, Singh UC, Weiner PK, Kollman PA. 1999. *AMBER 6*. San Francisco: University of California.

Cheong C, Varani G, Tinoco I Jr. 1990. Solution structure of an unusually stable RNA hairpin, 5′GGAC(UUCG)GUCC. *Nature 346*: 680–682.

Cotten M, Gick O, Vasserot A, Schaffner G, Birnstiel ML. 1988. Specific contacts between mammalian U7 snRNA and histone precursor RNA are indispensable for the in vitro 3′ RNA processing reaction. *EMBO J 7*:801–808.

DeJong ES, Marzluff WF, Nikonowicz EP. 2002. NMR structure and dynamics of the RNA binding site for the histone mRNA stem-loop binding protein. *RNA 8*:83–96.

Delaglio F, Grzesiek S, Vuister G, Zhu G, Pfeifer J, Bax A. 1995. NMRPipe: A multidimensional spectral processing system based on UNIX Pipes. *J Biomol NMR 6*:277–293.

Dingley AJ, Grzesiek S. 1998. Direct observation of hydrogen bonds in nucleic acid base pairs by internucleotide $^{2}J_{NN}$ couplings. *J Am Chem Soc 120*:8293–8297.

Dominski Z, Erkmann JA, Greenland JA, Marzluff WF. 2001. Mutations in the RNA binding domain of stem-loop binding protein define separable requirements for RNA binding and for histone pre-mRNA processing. *Mol Cell Biol 21*:2008–2017.

Dominski Z, Marzluff WF. 1999. Formation of the 3′ end of histone mRNA. *Gene 239*:1–14.

Dominski Z, Zheng LX, Sanchez R, Marzluff WF. 1999. Stem-loop binding protein facilitates 3′-end formation by stabilizing U7 snRNP binding to histone pre-mRNA. *Mol Cell Biol 19*:3561–3570.

Eckner R, Ellmeier W, Birnstiel ML. 1991. Mature mRNA 3′ end formation stimulates RNA export from the nucleus. *EMBO J 10*:3513–3522.

Fiala R, Czernek J, Sklenar V. 2000. Transverse relaxation optimized triple-resonance NMR experiments for nucleic acids. *J Biomol NMR 16*:291–302.

Freier SM, Kierzek R, Jaeger JA, Sugimoto N, Caruthers MH, Neilson T, Turner DH. 1986. Improved free-energy parameters for predictions of RNA duplex stability. *Proc Natl Acad Sci USA 83*:9373–9377.

Gallie DR, Lewis NJ, Marzluff WF. 1996. The histone 3′-terminal stem-loop is necessary for translation in Chinese hamster ovary cells. *Nucleic Acids Res 24*:1954–1962.

Gruber A, Streit A, Reist M, Benninger P, Bohni R, Schümperli D. 1990. Structure of a mouse histone-encoding gene cluster. *Gene 95*:303–304.

Gutell RR, Cannone JJ, Konings D, Gautheret D. 2000. Predicting U-turns in ribosomal RNA with comparative sequence analysis. *J Mol Biol 300*:791–803.

Hennig M, Williamson JR. 2000. Detection of N-H…N hydrogen bonding in RNA via scalar couplings in the absence of observable imino proton resonances. *Nucleic Acids Res 28*:1585–1593.

Heus HA, Wijmenga SS, van de Ven FJM, Hilbers CW. 1994. Sequential backbone assignment in ^{13}C-labeled RNA via through-bond coherence transfer using three-dimensional triple resonance spectroscopy (^{1}H, ^{13}C, ^{31}P) and two-dimensional TOCSY. *J Am Chem Soc 116*:4983–4984.

Jucker FM, Pardi A. 1995. Solution structure of the CUUG hairpin loop: A novel RNA tetraloop motif. *Biochemistry 34*:14416–14427.

Kellogg GW. 1992. Proton-detected hetero-TOCSY experiments with application to nucleic acids. *J Magn Reson 98*:176–182.

Legault P, Jucker FM, Pardi A. 1995. Improved measurement of ^{13}C, ^{31}P J coupling constants in isotopically labeled RNA. *FEBS Lett 362*:156–160.

Legault P, Pardi A. 1994. In situ probing of adenine protonation in RNA by ^{13}C NMR. *J Am Chem Soc 116*:8390–8391.

Linge JP, O'Donoghue SI, Nilges M. 2001. Automated assignment of ambiguous nuclear overhauser effects with ARIA. *Methods Enzymol 339*:71–90.

Luscombe NM, Austin SE, Berman HM, Thornton JM. 2001. An overview of the structures of protein–DNA complexes. *Genome Biol 1*:1–37.

Luy B, Marino JP. 2000. Direct evidence for Watson–Crick base pairs in a dynamic region of RNA structure. *J Am Chem Soc 122*:8095–8096.

Marino JP, Schwalbe H, Anklin C, Bermel W, Crothers DM, Griesinger C. 1995. Sequential correlation of anomeric ribose protons and intervening phosphorus in RNA oligonucleotides by a ^{1}H, ^{13}C, ^{31}P triple resonance experiment: HCP-CCH-TOCSY. *J Biomol NMR 5*:87–92.

Marino JP, Schwalbe H, Glaser SJ, Griesinger C. 1996. Determination of γ and stereospecific assignment of H5′ protons by measurement of ^{2}J and ^{3}J couplings constants in uniformly ^{13}C labeled RNA. *J Am Chem Soc 118*:4388–4395.

Markley JL, Bax A, Arata Y, Hilbers CW, Kaptein R, Sykes BD, Wright PE, Wüthrich K. 1998. Recommendations for the presentation of NMR structures of proteins and nucleic acids—IUPAC-IUBMB-IUPAB Inter-Union Task Group on the Standardization of Data Bases of Protein and Nucleic Acid Structures Determined by NMR Spectroscopy. *J Biomol NMR 12*:1–23.

Martin F, Michel F, Zenklusen D, Müller B, Schümperli D. 2000. Positive and negative mutant selection in the human histone hairpin-binding protein using the yeast three-hybrid system. *Nucleic Acids Res 28*:1594–1603.

Martin F, Schaller A, Eglite S, Schümperli D, Müller B. 1997. The gene for histone RNA hairpin binding protein is located on human chromosome 4 and encodes a novel type of RNA binding protein. *EMBO J 16*:769–778.

Marzluff WF. 1992. Histone 3′ ends: Essential and regulatory functions. *Gene Expr 2*:93–97.

Michel F, Schümperli D, Müller B. 2000. Specificities of *Caenorhabditis elegans* and human hairpin binding proteins for the first nucleotide in the histone mRNA hairpin loop. *RNA 6*:1539–1550.

Milligan JF, Groebe DR, Witherell GW, Uhlenbeck OC. 1987. Oligoribonucleotide synthesis using T7 RNA polymerase and synthetic DNA templates. *Nucleic Acids Res 15*:8783–8798.

Moore PB. 1999. Structural motifs in RNA. *Annu Rev Biochem 68*:287–300.
Mowry KL, Oh R, Steitz JA. 1989. Each of the conserved sequence elements flanking the cleavage site of mammalian histone pre-mRNAs has a distinct role in the 3′-end processing reaction. *Mol Cell Biol 9*:3105–3108.
Müller B, Schümperli D. 1997. The U7 snRNP and the hairpin binding protein: Key players in histone mRNA metabolism. *Semin Cell Dev Biol 8*:567–576.
Nilges M, O'Donoghue SI. 1998. Ambiguous NOEs and automated NOESY assignment. *Prog NMR Spectrosc 32*:107–139.
Osley MA. 1991. The regulation of histone synthesis in the cell cycle. *Annu Rev Biochem 60*:827–861.
Pandey NB, Marzluff WF. 1987. The stem-loop structure at the 3′ end of histone mRNA is necessary and sufficient for regulation of histone mRNA stability. *Mol Cell Biol 7*:4557–4559.
Pandey NB, Williams AS, Sun JH, Brown VD, Bond U, Marzluff WF. 1994. Point mutations in the stem-loop at the 3′ end of mouse histone mRNA reduce expression by reducing the efficiency of 3′ end formation. *Mol Cell Biol 14*:1709–1720.
Pardi A, Nikonowicz EP. 1992. Simple procedure for resonance assignment of the sugar protons in ^{13}C-labeled RNAs. *J Am Chem Soc 114*:9202–9203.
Price SR, Oubridge C, Varani G, Nagai K. 1998. Preparation of RNA:protein complexes for X-ray crystallography and NMR. In: CWJ Smith, ed. *RNA:protein interactions*. Oxford: Oxford University Press. pp 37–74.
Riesner D, Maass G, Thiebe R, Philippsen P, Zachau HG. 1973. The conformational transitions in yeast tRNA^{Phe} as studied with tRNA^{Phe} fragments. *Eur J Biochem 36*:76–88.
Saenger W. 1984. *Principles of nucleic acid structure*. New York: Springer.
Sattler M, Schleucher J, Griesinger C. 1999. Heteronuclear multidimensional NMR experiments for the structure determination of proteins in solution employing pulsed field gradients. *Prog NMR Spectrosc 34*:93–158.
Schaller A, Martin F, Müller B. 1997. Characterization of the calf thymus hairpin-binding factor involved in histone pre-mRNA 3′ end processing. *J Biol Chem 272*:10435–10441.
Schaufele F, Gilmartin GM, Bannwarth W, Birnstiel ML. 1986. Compensatory mutations suggest that base-pairing with a small nuclear RNA is required to form the 3′ end of H3 messenger RNA. *Nature 323*:777–781.
Schümperli D. 1988. Multilevel regulation of replication-dependent histone genes. *Trends Genet 4*:187–191.
Schwalbe H, Marino JP, Glaser SJ, Griesinger C. 1995. Measurement of H,H-coupling constants associated with ν_1, ν_2 and ν_3 in uniformly ^{13}C-labeled RNA by HCC-TOCSY-CCH-E.COSY. *J Am Chem Soc 117*:7251–7252.
Seeman NC, Rosenberg JM, Rich A. 1976. Sequence-specific recognition of double helical nucleic acids by proteins. *Proc Natl Acad Sci USA 73*:804–808.
Simon B, Zanier K, Sattler M. 2001. A TROSY relayed HCCH-COSY experiment for correlating adenine H2/H8 resonances in uniformly ^{13}C-labeled RNA molecules. *J Biomol NMR 20*:173–176.
Sklenar V, Dieckmann T, Butcher SE, Feigon J. 1996. Through-bond correlation of imino and aromatic resonances in ^{13}C-, ^{15}N-labeled RNA via heteronuclear TOCSY. *J Biomol NMR 7*:83–87.
Sklenar V, Dieckmann T, Butcher SE, Feigon J. 1998. Optimization of triple-resonance HCN experiments for application to larger RNA oligonucleotides. *J Magn Reson 130*:119–124.
Spycher C, Streit A, Stefanovic B, Albrecht D, Koning TH, Schumperli D. 1994. 3′ end processing of mouse histone pre-mRNA: Evidence for additional base-pairing between U7 snRNA and pre-mRNA. *Nucleic Acids Res 22*:4023–4030.
Stallings SC, Moore PB. 1997. The structure of an essential splicing element: Stem loop IIa from yeast U2 snRNA. *Structure 5*:1173–1185.
Streit A, Koning TW, Soldati D, Melin L, Schumperli D. 1993. Variable effects of the conserved RNA hairpin element upon 3′ end processing of histone pre-mRNA in vitro. *Nucleic Acids Res 21*:1569–1575.
Tsui V, Case DA. 2000. Molecular dynamics simulations of nucleic acids with a generalized Born solvation model. *J Am Chem Soc 122*:2489–2498.
Varani G, Aboul-ela F, Allain FH-T. 1996. NMR investigation of RNA structure. *Progr NMR Spectrosc 29*:51–127.
Wang ZF, Whitfield ML, Ingledue TC 3rd, Dominski Z, Marzluff WF. 1996. The protein that binds the 3′ end of histone mRNA: A novel RNA-binding protein required for histone pre-mRNA processing. *Genes & Dev 10*:3028–3040.
Whitfield ML, Zheng LX, Baldwin A, Ohta T, Hurt MM, Marzluff WF. 2000. Stem-loop binding protein, the protein that binds the 3′ end of histone mRNA, is cell cycle regulated by both translational and posttranslational mechanisms. *Mol Cell Biol 20*:4188–4198.
Wijmenga S, van Buuren BNM. 1998. The use of NMR methods for conformational studies of nucleic acids. *Progr NMR Spectrosc 32*:287–387.
Williams AS, Ingledue TC 3rd, Kay BK, Marzluff WF. 1994. Changes in the stem-loop at the 3′ terminus of histone mRNA affects its nucleocytoplasmic transport and cytoplasmic regulation. *Nucleic Acids Res 22*:4660–4666.
Wittop Koning TH, Schümperli D. 1994. RNAs and ribonucleoproteins in recognition and catalysis. *Eur J Biochem 219*:25–42.
Zimmer DP, Marino JP, Griesinger C. 1996. Determination of homo- and heteronuclear coupling constants in uniformly ^{13}C, ^{15}N-labeled DNA oligonucleotides. *Magn Reson Chem 34*:S177–S186.

APPENDIX

Tables A1 and A2 show chemical shifts and experimental J-couplings and torsion angles for the histone 3′ hairpin.

TABLE A1. Chemical shifts.

G1	P	—	C1′	92.64	5.78	C2′	74.60	4.90	C3′	73.03	4.78	C4′	83.22	4.49	C5′	65.58	4.41	4.16
	N9	—	C8	136.96	H8	7.49	N1	—	H1	—	N2	—	H21	—	H22	—		
G2	P	—	C1′	91.12	6.02	C2′	76.16	4.72	C3′	—	—	C4′	84.01	4.56	C5′	67.14	4.28	4.11
	N9	—	C8	137.35	H8	7.74	N1	147.58	H1	12.83	N2	—	H21	—	H22	—		
A3	P	—	C1′	92.07	5.79	C2′	76.16	4.51	C3′	74.60	4.80	C4′	83.62	4.50	C5′	65.75	4.48	4.20
	N9	—	C8	140.88	H8	8.16	N1	—	C2	—	H2	—	N6	—	H61	—	H62	—
A4	P	—	C1′	92.72	5.79	C2′	74.99	4.60	C3′	73.06	4.68	C4′	82.55	4.49	C5′	64.89	4.53	4.16
	N9	—	C8	140.09	H8	8.07	N1	—	C2	155.00	H2	8.11	N6	—	H61	—	H62	—
G5	P	—	C1′	92.64	5.75	C2′	75.38	4.44	C3′	72.24	4.52	C4′	81.66	4.46	C5′	64.79	4.53	4.12
	N9	—	C8	136.17	H8	7.43	N1	147.13	H1	12.44	N2	—	H21	—	H22	—		
G6	P	—	C1′	93.42	5.52	C2′	75.38	4.39	C3′	75.38	4.34	C4′	81.66	4.41	C5′	—	—	—
	N9	—	C8	140.96	H8	7.69	N1	148.72	H1	13.45	N2	—	H21	—	H22	—		
C7	P	−4.18	C1′	93.42	5.51	C2′	75.38	4.39	C3′	71.85	4.42	C4′	81.66	4.41	C5′	64.40	4.38	4.03
	N1	—	C6	140.88	H6	7.69	C5	96.95	H5	5.19	N3	197.36	N4	102.02	H41	8.80	H42	6.99
C8	P	−4.28	C1′	93.81	5.49	C2′	75.38	4.38	C3′	71.85	4.42	C4′	81.66	4.41	C5′	64.40	4.51	4.06
	N1	—	C6	141.27	H6	7.77	C5	97.74	H5	5.49	N3	197.21	N4	100.98	H41	8.75	H42	7.07
C9	P	−4.44	C1′	93.81	5.48	C2′	75.38	4.34	C3′	71.85	4.42	C4′	81.66	4.38	C5′	64.46	4.52	4.05
	N1	—	C6	141.27	H6	7.75	C5	97.74	H5	5.48	N3	196.27	N4	100.84	H41	8.67	H42	7.03
U10	P	−4.36	C1′	92.64	5.72	C2′	75.79	4.40	C3′	73.03	4.51	C4′	82.83	4.34	C5′	64.79	4.45	4.05
	N1	—	C6	141.66	H6	7.70	C5	103.62	H5	5.44	N3	163.85	H3	13.91				
U11	P	−4.24	C1′	91.85	5.58	C2′	74.99	4.24	C3′	74.99	4.43	C4′	84.01	4.30	C5′	66.75	4.19	3.98
	N1	—	C6	143.62	H6	7.74	C5	104.80	H5	5.77	N3	—	H3	—				
U12	P	−3.88	C1′	89.53	5.87	C2′	74.99	4.38	C3′	77.34	4.40	C4′	85.97	4.30	C5′	67.54	4.02	3.95
	N1	—	C6	143.62	H6	7.75	C5	105.58	H5	5.87	N3	—	H3	—				
U13	P	−3.74	C1′	89.89	5.44	C2′	75.81	4.13	C3′	76.95	4.46	C4′	84.79	3.93	C5′	67.54	3.93	3.86
	N1	—	C6	142.84	H6	7.32	C5	105.19	H5	5.65	N3	—	H3	—				
C14	P	−4.18	C1′	91.07	6.00	C2′	75.79	4.46	C3′	76.16	4.54	C4′	84.01	4.56	C5′	67.16	4.28	4.11
	N1	—	C6	143.23	H6	7.85	C5	98.91	H5	5.87	N3	—	N4	—	H41	—	H42	—
A15	P	−4.20	C1′	93.04	5.95	C2′	75.43	4.72	C3′	73.42	4.64	C4′	82.80	4.57	C5′	66.38	4.43	4.25
	N9	—	C8	140.49	H8	8.39	N1	147.32	C2	153.43	H2	7.60	N6	—	H61	—	H62	—
G16	P	−4.40	C1′	92.26	5.67	C2′	75.38	4.54	C3′	72.24	4.52	C4′	81.69	4.45	C5′	65.32	4.53	4.11
	N9	—	C8	136.17	H8	7.43	N1	147.92	H1	12.91	N2	—	H21	—	H22	—		
G17	P	−4.15	C1′	92.64	5.79	C2′	75.38	4.55	C3′	72.64	4.52	C4′	81.66	4.48	C5′	64.79	4.53	4.08
	N9	—	C8	135.78	H8	7.26	N1	148.72	H1	12.98	N2	—	H21	—	H22	—		
G18	P	−4.20	C1′	92.64	5.77	C2′	74.99	4.44	C3′	72.24	4.51	C4′	81.66	4.46	C5′	64.79	4.54	4.07
	N9	—	C8	135.78	H8	7.30	N1	30.46	H1	13.46	N2	—	H21	—	H22	—		
C19	P	−4.49	C1′	93.42	5.52	C2′	75.38	4.41	C3′	71.85	4.42	C4′	81.66	4.41	C5′	64.40	4.53	4.06
	N1	—	C6	140.88	H6	7.67	C5	96.95	H5	5.18	N3	197.44	N4	102.02	H41	8.81	H42	7.00
C20	P	−4.06	C1′	93.81	5.50	C2′	75.38	4.51	C3′	72.24	4.49	C4′	81.66	4.41	C5′	64.40	4.52	4.08
	N1	—	C6	140.88	H6	7.67	C5	97.74	H5	5.47	N3	195.80	N4	100.57	H41	8.53	H42	7.07
A21	P	−4.00	C1′	92.64	5.92	C2′	76.14	4.49	C3′	73.81	4.59	C4′	82.83	4.53	C5′	65.58	4.52	4.15
	N9	—	C8	139.31	H8	8.05	N1	—	C2	—	H2	—	N6	—	H61	—	H62	—
C22	P	−4.24	C1′	93.81	5.13	C2′	75.40	4.20	C3′	71.85	4.32	C4′	81.66	4.33	C5′	64.40	4.46	4.06
	N1	—	C6	140.88	H6	7.46	C5	96.95	H5	5.24	N3	—	N4	—	H41	—	H42	—
C23	P	−4.36	C1′	93.81	5.37	C2′	75.38	4.23	C3′	72.24	4.35	C4′	81.66	4.32	C5′	64.73	4.47	4.04
	N1	—	C6	141.27	H6	7.70	C5	97.74	H5	5.57	N3	—	N4	100.40	H41	8.39	H42	7.08
C24	P	−4.18	C1′	92.64	5.64	C2′	77.34	3.92	C3′	69.50	4.10	C4′	83.62	4.10	C5′	64.79	4.37	3.98
	N1	—	C6	141.66	H6	7.66	C5	97.74	H5	5.57	N3	—	N4	—	H41	—	H42	—

^{1}H, ^{15}N, and ^{13}C chemical shifts are referenced to H_2O, liquid NH_3, and DSS, respectively (Markley, 1998).

TABLE A2. Experimental J-couplings and torsion angles for the histone 3′ hairpin.

	U10	U11	U12	U13	C14	A15
Experimental J-couplings for residues 10–15[a]						
$^3J_{(H1', H2')}$	1.9	3.9	8.5	7.0	6.8	<1.0
$^3J_{(H3', H4')}$	7.0	5.8	1.5	2.5	n.d.	9.0
Pucker	**N**		**S**	**S**		**N**
$^3J_{(H4', H5')}$	3.0	<1.0	3.0	<1.0	3.0	2.0
$^3J_{(H4', H5'')}$	2.0	3.0	<1.0	2.0	<1.0	2.0
γ	**g$^+$**	g$^+$	**g$^+$**	**g$^+$**	g$^+$	**g$^+$**
$^3J_{(C2', P)}$	4.2	4.4	6.0	5.5	4.4	<1.0
ϵ	**t/g$^-$**	**t/g$^-$**	**g$^-$**	**g$^-$**	**t/g$^-$**	t
Torsion angles for residues 10–15 in the final NMR ensemble[b]						
α	−75 ± 1	−59 ± 3	74 ± 60	−64 ± 3	51 ± 92	−89 ± 19
β	177 ± 2	169 ± 3	−139 ± 57	154 ± 4	−170 ± 67	151 ± 9
γ	71 ± 2	73 ± 1	66 ± 10	37 ± 3	119 ± 45	74 ± 7
δ	85 ± 2	132 ± 1	103 ± 5	154 ± 4	96 ± 22	77 ± 3
χ	−138 ± 1	−154 ± 2	−111 ± 10	−144 ± 6	−123 ± 27	−175 ± 8
ϵ	−164 ± 1	−80 ± 29	−76 ± 1	−83 ± 37	−169 ± 41	−157 ± 6
ζ	−79 ± 1	106 ± 52	−151 ± 7	131 ± 52	32 ± 42	−75 ± 2

[a]Sugar conformations (pucker) predicted by the J-couplings are labeled N or S, and the γ and ϵ conformations consistent with the experimentally determined J-couplings are shown. Torsion angles that were restrained during the structure calculations (as described in Materials and Methods) are highlighted in bold.

[b]Torsion angles in the final ensemble of NMR structures.